PHILOSOPHICAL TRANSACTIONS OF THE ROYAL SOCIETY A

Phil. Trans. R. Soc. A (2011) **369**, 2779–2799
doi:10.1098/rsta.2011.0072

Review

Functional renormalization for the Bardeen–Cooper–Schrieffer to Bose–Einstein condensation crossover

By Michael M. Scherer[1], Stefan Floerchinger[2] and Holger Gies[1,*]

[1] *Theoretisch-Physikalisches Institut, Friedrich-Schiller-Universität Jena, Max-Wien-Platz 1, 07749 Jena, Germany*
[2] *Institut für Theoretische Physik, Universität Heidelberg, Philosophenweg 16, 69120 Heidelberg, Germany*

We review the functional renormalization group (RG) approach to the Bardeen–Cooper–Schrieffer to Bose–Einstein condensation (BCS–BEC) crossover for an ultracold gas of fermionic atoms. Formulated in terms of a scale-dependent effective action, the functional RG interpolates continuously between the atomic or molecular microphysics and the macroscopic physics on large length scales. We concentrate on the discussion of the phase diagram as a function of the scattering length and the temperature, which is a paradigm example for the non-perturbative power of the functional RG. A systematic derivative expansion provides for both a description of the many-body physics and its expected universal features as well as an accurate account of the few-body physics and the associated BEC and BCS limits.

Keywords: functional renormalization group; ultracold fermionic atoms; Bardeen–Cooper–Schrieffer to Bose–Einstein condensation crossover

1. Introduction

Many challenges in contemporary theoretical physics deal with strongly interacting quantum field theories or many-body systems. Progress often relies on the construction of exact or approximate solutions. In the absence of exact solutions, reliable and controlled approximation methods typically are the only source of information about the system and the underlying physical mechanisms. An approximation scheme may be considered as reliable and controlled if it is based on a systematic and consistent expansion scheme and shows convergence towards the exact result (which, however, is often not known). Textbook examples are, of course, provided by perturbative expansions or lattice discretizations, both

*Author for correspondence (gies@tpi.uni-jena.de).

One contribution of 11 to a Theme Issue 'New applications of the renormalization group in nuclear, particle and condensed matter physics'.

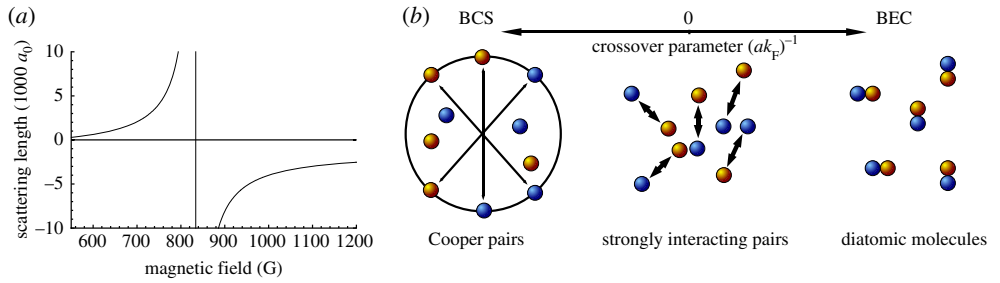

Figure 1. (*a*) Schematic plot of a Feshbach resonance, e.g. O'Hara *et al.* [3]. (*b*) Sketch of the cross over physics. (Online version in colour.)

of which can be consistently evaluated to a given order or lattice refinement and systematically improved, and the convergence can at least be checked as a matter of practice.

In this contribution, we would like to demonstrate that the functional renormalization group (RG) can be used to develop systematic and consistent expansion schemes for strongly interacting systems. Most importantly, it can be applied in the space–time continuum and does not require a perturbative ordering scheme. Nevertheless, it offers a variety of tools to verify qualitative and quantitative reliability and practical convergence. As a prime example of strongly interacting many-body systems, we take the Bardeen–Cooper–Schrieffer (BCS) to Bose–Einstein condensation (BEC) crossover as an illustration for the use of the functional RG. The concrete physical system that we have in mind is an ultracold atomic Fermi gas with two accessible hyperfine spin states near a Feshbach resonance, showing a smooth crossover between BCS superfluidity and BEC of diatomic molecules [1,2].

By means of an external magnetic field B, the phenomenon of a Feshbach resonance allows one to arbitrarily regulate the effective interaction strength of the atoms, parametrized by the s-wave scattering length a. We briefly discuss the example of ^{6}Li [3], which besides ^{40}K has been realized in current experiments [4–9] (figure 1*a*).

For magnetic fields larger than approximately 1200 G, the scattering length a is small and negative, giving rise to the many-body effect of Cooper pairing and a BCS-type ground state below a critical temperature. The BCS ground state is a superfluid described by a non-vanishing order parameter $\phi_0 = \langle \psi_1, \psi_2 \rangle$ bilinear in the fermion fields. An increase of the temperature leads to a second-order phase transition to a normal fluid, $\phi_0 = 0$. Magnetic fields below $B \sim 600\,\mathrm{G}$ induce a small and positive scattering length a and the formation of a diatomic bound state, a dimer. The ground state is a BEC of repulsive dimers, and again a phase transition from a superfluid, $\phi_0 > 0$, to a normal fluid, $\phi_0 = 0$, can be observed at a critical temperature. For magnetic fields in the regime $700\,\mathrm{G} \lesssim B \lesssim 1100\,\mathrm{G}$, the modulus of the scattering length $|a|$ is large and diverges at the *unitary point*, $B_0 = 834\,\mathrm{G}$, where unitarity of the scattering matrix solely determines the two-body scattering properties. At and near unitarity, the fermions are in a strongly interacting regime. It connects the limits of BCS superfluidity and BEC by a continuous crossover and also shows a superfluid ground state, with $\phi_0 > 0$ [1,2].

A convenient parametrization of the crossover is given by the quantity $c^{-1} = (ak_F)^{-1}$. Here the density of atoms

$$n = \frac{k_F^3}{3\pi^2} \tag{1.1}$$

defines the formal Fermi momentum k_F in natural units with $\hbar = k_B = 2M = 1$, where M is the mass of the atoms. We emphasize that k_F is defined by equation (1.1) for all values of the scattering length a and the temperature T. Except in the limit $a \to 0_-$ at $T = 0$, k_F is not related to the size of the Fermi sphere but merely parametrizes the momentum scale associated with the particle number density. Up to a numerical factor, the parameter c measures the scattering length in units of the typical inter-particle distance. Its inverse c^{-1} varies from large negative values on the BCS side to large positive values on the BEC side, with a zero-crossing at the unitary point (figure 1*b*).

A description of the qualitative features of the BCS–BEC crossover has been achieved by Nozieres & Schmitt-Rink [10] and Sa de Melo *et al.* [11] within extended mean-field theories, which account for the contribution of both fermionic and bosonic degrees of freedom. However, the quantitatively precise understanding of BCS–BEC crossover physics requires non-perturbative methods. The experimental realization of molecule condensates and the subsequent crossover to a BCS-like state of weakly attractive fermions [4–9] pave the way to future experimental precision measurements and provide a testing ground for non-perturbative methods. An understanding of the crossover on a quantitative level at and near the resonance has been developed through numerical quantum Monte Carlo (QMC) methods [12–16]. The complete phase diagram has been accessed by functional field-theoretical techniques, such as t-matrix approaches [17,18], Dyson–Schwinger equations [19], two-particle irreducible (2PI) methods [20] and RG flow equations [21–26]. These pictures of the whole phase diagram [17–24,27] do not yet reach a similar quantitative precision as anticipated for the QMC calculations.

We intend to fill this gap and discuss the limit of broad Feshbach resonances, for which all thermodynamic quantities can be expressed in terms of two dimensionless parameters,

$$c = ak_F \quad \text{and} \quad \frac{T}{T_F}, \tag{1.2}$$

the latter being the temperature in units of the Fermi temperature $T_F = k_F^2$. In the broad resonance regime, macroscopic observables are *universal* [19,22,27,28], i.e. they are to a large extent independent of the concrete microscopic realization. Very similar to the notion of universality near second-order phase transitions, universality in the present context can be traced back to the existence of a fixed point in the RG flow, which is approached provided the Feshbach (Yukawa) coupling is large enough [23].

Our review is based on previous studies of RG [22,23,29–31]. Certain authors study RG using different expansion schemes [21,24–26]. In the following, we first introduce the required techniques from RG flow equations for cold atoms (see §2). Further, we include the quantitative effect of particle–hole (ph) fluctuations (§4),

and systematically extend the truncation scheme, accounting for changes in the Fermi surface due to fluctuation effects (§5). Additionally, we also consider an atom–dimer interaction term.

2. Microscopic model and the functional renormalization group

Microscopically, the BCS–BEC crossover can be described by a fermionic action including a self-interacting two-component Grassmann field, $\psi = (\psi_1, \psi_2)$, describing non-relativistic fermions in two hyperfine states. In thermal equilibrium, the system is described by the Matsubara formalism,

$$S = \int_0^{1/T} \mathrm{d}\tau \int \mathrm{d}^3x \{\psi^\dagger(\partial_\tau - \nabla^2 - \mu)\psi\} + S_{\mathrm{int}}, \tag{2.1}$$

with μ denoting the chemical potential, the atom mass M being set to $2M = 1$ and

$$S_{\mathrm{int}} = \int_{p_1,p_2,p_1',p_2'} \lambda_{\psi,\mathrm{eff}}(p_1 + p_2)\psi_1^*(p_1')\psi_1(p_1)\psi_2^*(p_2')\psi_2(p_2)\delta(p_1 + p_2 - p_1' - p_2'), \tag{2.2}$$

where $p = (p_0, \boldsymbol{p})$. In the limit of broad Feshbach resonances, the microscopic interaction can be well approximated as point-like, $\lambda_{\psi,\mathrm{eff}} \sim \mathrm{const}$. More generally, we expect the occurrence of composite bosonic degrees of freedom that can manifest themselves as poles of the fermionic four-point correlator. In the following, we parametrize such a pole by

$$\lambda_{\psi,\mathrm{eff}}(q) = -\frac{h_\Lambda^2}{-\omega + (\boldsymbol{q}^2/2) - 2\mu + \nu_\Lambda(B)}, \tag{2.3}$$

where ω is the real-time frequency of the exchanged boson ϕ. It is related to the Matsubara frequency q_0 via analytical continuation, $\omega = -\mathrm{i}q_0$. Further, $\boldsymbol{q} = \boldsymbol{p}_1 + \boldsymbol{p}_2$ is the centre-of-mass momentum of the scattering fermions ψ_1 and ψ_2 with momenta $\boldsymbol{p}_1$ and $\boldsymbol{p}_2$, respectively. In the presence of a chemical potential, the pole is shifted by 2μ as the composite bosons carry atom number 2. The same factor occurs in front of the kinetic term, as the boson carries mass $2M$. The parameter $\nu_\Lambda(B) = \nu(B) + \delta\nu(\Lambda)$ includes the detuning from the Feshbach resonance $\nu(B) = \mu_{\mathrm{M}}(B - B_0)$, with the magnetic moment of the boson field μ_{M}, and a renormalization counter-term $\delta\nu(\Lambda)$. The latter has to be adjusted to match the conditions from the physical vacuum, as discussed below.

By means of a Hubbard–Stratonovich transformation, the action can be shown to be equivalent to a mixed fermionic/bosonic theory with the action

$$S = \int_0^{1/T} \mathrm{d}\tau \int d^3x \left\{\psi^\dagger(\partial_\tau - \nabla^2 - \mu)\psi + \phi^* \left(\partial_\tau - \frac{\nabla^2}{2} - 2\mu + \nu_\Lambda(B)\right)\phi \right.$$
$$\left. - h_\Lambda(\phi^*\psi_1\psi_2 + \mathrm{h.c.})\right\}. \tag{2.4}$$

Here, the complex scalar field ϕ parametrizes the bosonic degrees of freedom. In different regimes of the crossover, ϕ can be seen as a field describing molecules, Cooper pairs or simply an auxiliary field. The equivalance of this action to the

purely fermionic description can be seen by inserting the equations of motion for the boson field on the classical level. This corresponds to a Gaussian functional integration of the boson field on the quantum level.

The Yukawa coupling h_Λ is related to the width of the Feshbach resonance. In the formal limit of $h_\Lambda \to \infty$ with h_Λ^2/ν_Λ fixed, the microscopic interaction becomes point-like (momentum and frequency independent) again with strength $-h_\Lambda^2/\nu_\Lambda$, as expected for broad Feshbach resonances.

The above theory is considered to provide for a model of fermionic atomic gases at a *microscopic* scale (a UV momentum scale Λ), say on length scales of a few times the Bohr radius or the van der Waals length. For bridging the gap towards the long-range behaviour, we use the functional RG. The functional RG can be formulated as a functional differential equation for an action functional for which the microscopic model serves as an initial value. Whereas the microscopic interactions are governed by S of equation (2.4) at the UV scale Λ, quantum and thermal fluctuations effectively modify the interactions at larger length scales, which can be summarized in an effective action Γ_k (e.g. for the one-particle irreducible proper vertices) valid at a momentum scale k. In other words, Γ_k includes the effects of fluctuations with momenta higher than k and governs the interactions with momenta near k. This *effective average action* or *flowing action* satisfies the Wetterich equation [32], being an exact RG flow equation,

$$\partial_k \Gamma_k[\Phi] = \frac{1}{2}\mathrm{STr}[(\Gamma_k^{(2)}[\Phi] + R_k)^{-1}\partial_k R_k]. \tag{2.5}$$

Here, the STr operation involves an integration over momenta and a summation over internal indices with appropriate minus signs for fermions. The collective field Φ summarizes all bosonic and fermionic degrees of freedom, and $\Gamma_k^{(2)}[\Phi]$ denotes the second functional derivative of Γ_k,

$$(\Gamma_k^{(2)}[\Phi])_{ij}(p_1, p_2) = \frac{\vec{\delta}}{\delta\Phi_i(-p_1)}\Gamma_k[\Phi]\frac{\overleftarrow{\delta}}{\delta\Phi_j(p_2)}. \tag{2.6}$$

The long-wavelength regulator R_k specifies the details of the regularization scheme. Specific examples will be discussed below. For reviews of the functional RG see [33–37]. From the full effective action in the long-wavelength limit $\Gamma[\Phi] = \Gamma_{k=0}[\Phi]$, all macroscopic properties of the system under consideration can be read off.

Equation (2.5) is the technical starting point of our investigations. It is a functional differential equation, which, upon expansion of this functional into a suitable basis, translates to a system of infinitely many coupled differential equations for the expansion coefficients, i.e. generalized running couplings. Identifying suitable expansion schemes is not a formal but a physics problem: expansions should be based on building blocks that encode the relevant degrees of freedom of the system possibly at all scales. In the present context, this emphasizes the usefulness of composite bosonic fields, which are expected to be the relevant long-range degrees of freedom at low temperatures. Reducing the full effective action to a treatable selection of generalized couplings defines a *truncation*. Possible truncation schemes include vertex expansions, derivative

expansions or other schemes to systematically classify all possible operators of a given system. The quantitative success of a given truncation scheme does not necessarily rely on the existence of a small expansion parameter like the interaction strength, but only requires that the operators neglected in a truncation do not have a strong dependence on the flow of the operators included. In practice, a truncation can be tested in various ways, e.g., by verifying the practical convergence for increasing truncations or by studying regulator-scheme independence for universal quantities. In the present context, also the comparison with well-known few-body physics turns out to provide a useful benchmark.

3. Basic truncation

(a) *Derivative expansion*

Thermodynamics of a system can be obtained from its grand canonical partition function Z or the corresponding grand canonical potential, $\Omega_{\mathrm{G}} = -T \ln Z$. It is related to the effective action via $\Gamma[\Phi_{\mathrm{eq}}] = \Omega_{\mathrm{G}}/T$, where Φ_{eq} is obtained from the field equation $(\delta/\delta\Phi)\Gamma[\Phi]|_{\Phi=\Phi_{\mathrm{eq}}} = 0$. Let us first present a basic version of a truncation that already captures all the qualitative features of the BCS–BEC crossover:

$$\Gamma_k[\Phi] = \int_{\tau,\boldsymbol{x}} \Big\{ \psi^\dagger(\partial_\tau - \nabla^2 - \mu)\psi + \bar{\phi}^* \left(\bar{Z}_\phi \partial_\tau - \frac{A_\phi \nabla^2}{2} \right) \bar{\phi} + \bar{U}(\bar{\rho}, \mu) - \bar{h}(\bar{\phi}^* \psi_1 \psi_2 + \bar{\phi} \psi_2^* \psi_1^*) \Big\}. \tag{3.1}$$

The effective potential $\bar{U}(\bar{\rho}, \mu)$ is a function of $\bar{\rho} = \bar{\phi}^* \bar{\phi}$ and μ. This truncation can be motivated by a systematic derivative expansion and an analysis of the symmetries encoded in Ward identities [22,29]. It does not yet incorporate, for instance, the effects of ph fluctuations and we will come back to this issue in §4. We define renormalized fields $\phi = A_\phi^{1/2} \bar{\phi}$, $\rho = A_\phi \bar{\rho}$ and renormalized couplings $Z_\phi = \bar{Z}_\phi / A_\phi$, $h = \bar{h}/\sqrt{A_\phi}$, and express equation (3.1) in these quantities:

$$\Gamma_k[\Phi] = \int_{\tau,\boldsymbol{x}} \Big\{ \psi^\dagger(\partial_\tau - \nabla^2 - \mu)\psi + \phi^* \left(Z_\phi \partial_\tau - \frac{\nabla^2}{2} \right) \phi + U(\rho, \mu) - h\,(\phi^* \psi_1 \psi_2 + \phi \psi_2^* \psi_1^*) \Big\}. \tag{3.2}$$

In the grand canonical formalism, the chemical potential μ is kept fixed, and the physical particle number density n is a result to be read off from $n = -\partial U/\partial\mu$ in the limit $k \to 0$. At finite k, we are thus dealing with a flowing density n_k, which approaches the physical density only for $k \to 0$. As we finally want to measure all the results in units set by the physical density n, we have to determine the value of the chemical potential $\mu = \mu_0$ that corresponds to the desired density. In practice, we expand the effective potential around the k-dependent location of the minimum $\rho_0(k)$ and the k-independent value of the chemical potential μ_0. We determine $\rho_0(k)$ and μ_0 by the requirements $(\partial_\rho U)(\rho_0(k), \mu_0) = 0$ for all k,

and $-(\partial_\mu U)(\rho_0,\mu_0)=n$ at $k=0$. More explicitly, we employ a simple expansion for $U(\rho,\mu)$ of the form

$$U(\rho,\mu)=U(\rho_0,\mu_0)-n_k(\mu-\mu_0)+(m^2+\alpha(\mu-\mu_0))(\rho-\rho_0)+\frac{1}{2}\lambda(\rho-\rho_0)^2. \tag{3.3}$$

In the symmetric or normal gas phase, we have $\rho_0=0$, while in the phase with spontaneous breaking of U(1) symmetry (superfluid phase), we have $\rho_0>0$ and $m^2=0$. The atom density $n=-\partial U/\partial\mu$ corresponds to n_k in the limit $k\to 0$.

The running couplings in this truncation explicitly are $m^2(k)$, $\lambda(k)$, $\alpha(k)$, n_k, $Z_\phi(k)$ and $h(k)$. In the phase with spontaneous symmetry breaking, m^2 is traded for ρ_0. In addition, we need the anomalous dimension $\eta=-k\partial_k \ln A_\phi$. At the microscopic scale $k=\Lambda$, the initial values of our couplings are determined from equation (2.4). This gives $m^2(\Lambda)=\nu_\Lambda(B)-2\mu$, $\rho_0(\Lambda)=0$, $\lambda(\Lambda)=0$, $Z_\phi(\Lambda)=1$, $h(\Lambda)=h_\Lambda$, $\alpha(\Lambda)=-2$ and $n_\Lambda=3\pi^2\mu\,\theta(\mu)$. Finally, our regularization scheme is specified by a regulator for space-like momenta, which for the fermionic and bosonic field components reads

$$R_{k,\psi}=[\mathrm{sign}(\boldsymbol{p}^2-\mu)k^2-(\boldsymbol{p}^2-\mu)]\theta(k^2-|\boldsymbol{p}^2-\mu|)$$

and

$$R_{k,\phi}=A_\phi\left(k^2-\frac{\boldsymbol{p}^2}{2}\right)\theta\left(k^2-\frac{\boldsymbol{p}^2}{2}\right),$$

respectively. For the fermions, it regularizes fluctuations around a fixed Fermi surface (effects due to the running of the Fermi surface will be discussed in §5), whereas bosonic fluctuations are suppressed for generic small momenta. This choice is optimized in the spirit of Litim [38] and Pawlowski [36].

For our choice of the regulator and with the basic approximation scheme in equation (3.2), the flow equation for the effective potential can be computed in a straightforward manner:

$$\begin{aligned}k\partial_k U=\eta\rho U'+\frac{\sqrt{2}k^5}{3\pi^2 Z_\phi}\left(1-\frac{2\eta}{5}\right)s_{\mathrm{B}}^{(0)}-\frac{k^4}{3\pi^2}\big((\mu+k^2)^{3/2}\theta(\mu+k^2)\\ -(\mu-k^2)^{3/2}\theta(\mu-k^2)\big)s_{\mathrm{F}}^{(0)},\end{aligned} \tag{3.4}$$

with the threshold functions

$$\begin{aligned}s_{\mathrm{B}}^{(0)}=\left(\sqrt{\frac{k^2+U'}{k^2+U'+2\rho U''}}+\sqrt{\frac{k^2+U'+2\rho U''}{k^2+U'}}\right)\\ \times\left(\frac{1}{2}+N_{\mathrm{B}}\left[\frac{\sqrt{k^2+U'}\sqrt{k^2+U'+2\rho U''}}{Z_\phi}\right]\right),\end{aligned} \tag{3.5}$$

and

$$s_{\mathrm{F}}^{(0)}=\frac{2}{\sqrt{k^4+h^2\rho}}\left(\frac{1}{2}-N_{\mathrm{F}}\left[\sqrt{k^4+h^2\rho}\right]\right). \tag{3.6}$$

The threshold functions exhibit a temperature dependence via the Bose and Fermi functions, $N_{\mathrm{B/F}}[\epsilon] = (\mathrm{e}^{\epsilon/T} \mp 1)^{-1}$. From the effective potential flow, we derive the flow equations for the running couplings m^2 or ρ_0 and λ. For details, we refer to Diehl *et al.* [29]. Further, we need flow equations for A_ϕ and Z_ϕ, which are obtained by the projections

$$\partial_t \bar{Z}_\phi = -\partial_t \frac{\partial}{\partial q_0}(\bar{P}_\phi)_{12}(q_0, 0)\bigg|_{q_0=0} \quad \text{and} \quad \partial_t A_\phi = 2\partial_t \frac{\partial}{\partial \boldsymbol{q}^2}(\bar{P}_\phi)_{22}(0, \boldsymbol{q})\bigg|_{\boldsymbol{q}=0}, \tag{3.7}$$

with the momentum-dependent part of the propagator

$$\frac{\delta^2 \Gamma_k}{\delta\bar{\phi}_i(q)\delta\bar{\phi}_j(q')}\bigg|_{\bar{\phi}_1=\sqrt{2\bar{\rho}_0},\,\bar{\phi}_2=0} = (\bar{P}_\phi)_{ij}(q)\delta(q+q'). \tag{3.8}$$

Here the boson field is expressed on the basis of real fields $\bar{\phi}(x) = (1/\sqrt{2})(\bar{\phi}_1(x) + \mathrm{i}\bar{\phi}_2(x))$. These flow equations are derived by Diehl *et al.* [29] and have a rather involved structure. Finally, we need the flow of the Yukawa coupling. In the symmetric regime, the loop contribution vanishes and the flow is given by the anomalous dimension,

$$\partial_t h = \frac{1}{2}\eta h, \quad \text{or in dimensionless units} \quad \partial_t \tilde{h}^2 = (-1+\eta)\tilde{h}^2, \tag{3.9}$$

where $\tilde{h}^2 = h^2/k$. In the regime of spontaneous symmetry breaking ($\rho_0 > 0$), there is a loop contribution $\sim h^3\lambda\rho_0$ from a mixed diagram involving both fermions and bosons. This contribution is quantitatively subleading, which we have also verified numerically. For the basic approximation scheme, equation (3.2), we therefore dropped this contribution.

(*b*) *Vacuum limit and contact to experiment*

The vacuum limit allows us to make contact with the experiment. We find that for $n = T = 0$, the crossover at finite density turns into a second-order phase transition in vacuum [27,39] as a function of the initial value $m^2(\Lambda)$. In order to see this, we consider the momentum-independent parts in both the fermion and the boson propagator, $-\mu$ (the 'chemical potential' for the fermions in vacuum) and $m(k=0)^2$, which act as gaps for the propagation of fermions and bosons. We find the following constraints, separating two different branches of the physical vacuum [39],

$$\left.\begin{aligned} &m^2(0) > 0, \quad \mu = 0 \quad \text{atom phase} \qquad (a^{-1} < 0),\\ &m^2(0) = 0, \quad \mu < 0 \quad \text{molecule phase} \quad (a^{-1} > 0)\\ \text{and} \quad &m^2(0) = 0, \quad \mu = 0 \quad \text{resonance} \qquad (a^{-1} = 0). \end{aligned}\right\} \tag{3.10}$$

The initial values $m^2(\Lambda)$ and h_Λ can be connected to the two-particle scattering in vacuum close to a Feshbach resonance. For this purpose, one follows the flow of $m^2(k)$ and $h(k)$ in vacuum, e.g. for negative scattering length $a^{-1} < 0$, i.e. $\mu = T = n = 0$, and extracts the renormalized parameters $m^2 = m^2(k=0)$, $h = h(k=0)$.

They have to match the physical conditions formulated in equation (3.10). We obtain the two relations

$$\bar{m}^2(\Lambda) = \mu_{\mathrm{M}}(B - B_0) - 2\mu + \frac{\bar{h}^2_\Lambda}{6\pi^2}\Lambda \quad \text{and} \quad a = -\frac{h^2(k=0)}{8\pi m^2(k=0)} = -\frac{\bar{h}^2(\Lambda)}{8\pi\mu_{\mathrm{M}}(B - B_0)}, \tag{3.11}$$

where μ_{M} is the relative magnetic moment of the molecules. These relations fix the initial conditions of our model completely and similar reasoning confirms their validity on the BEC side. Now, we can express the parameters $m^2(\Lambda)$ and $h^2(\Lambda)$ by the experimentally accessible quantities, $B - B_0$ and a. They remain valid also for non-vanishing density and temperature, as long as the UV cutoff Λ is much larger than T and μ.

(*c*) *Many-body phase diagram*

Although our flow equations describe accurately the vacuum limit and can be used to determine interesting few-body parameters, they are not restricted to that limit. In fact, for non-zero temperature and density, the flow deviates from its vacuum form at scales with $k^2 < T$ or $k^2 < T_{\mathrm{F}}$. The resulting system of ordinary coupled differential equations is then solved numerically for different chemical potentials μ and temperatures T. For temperatures sufficiently small compared with the Fermi temperature, $T/T_{\mathrm{F}} \ll 1$, we find that the effective potential U at the macroscopic scale $k = 0$ develops a minimum at a non-zero field value $\rho_0 > 0$, $\partial_\rho U(\rho_0) = 0$. The system is then in the superfluid phase. For larger temperatures, we find that the minimum is at $\rho_0 = 0$ and that the 'mass parameter' m^2 is positive, $m^2 = \partial_\rho U(0) > 0$. The critical temperature T_{c} of this phase transition between the superfluid and the normal phase is then defined as the temperature where

$$\rho_0 = 0, \quad \partial_\rho U(0) = 0 \quad \text{at} \quad k = 0. \tag{3.12}$$

Throughout the whole crossover, the transition $\rho_0 \to 0$ is continuous as a function of T, demonstrating that the phase transition is of second order. An analysis of the scaling of the correlation length confirms that the phase transition is governed by a Wilson–Fisher fixed point for the $N = 2$ universality class throughout the crossover [29]. This reflects the fact that the symmetries are properly encoded also on the level of the truncated action.

From the flow equations together with the initial conditions, we can already recover all the qualitative features of the BCS–BEC crossover, e.g. compute the phase diagram for the phase transition to superfluidity. The result for this basic approximation is displayed by the dot-dashed line in the figure in §6*b*.

(*d*) *Fixed point and universality*

In the vacuum limit and in the regime where $k^2 \gg -\mu$, the flow of the anomalous dimension reads $\eta = h^2/(6\pi^2 k)$ [29]. Together with the dimensionless flow of the Yukawa coupling, equation (3.9), this reveals the existence of an IR-attractive fixed point given by $\eta = 1$, $\tilde{h}^2 = 6\pi^2$. This fixed point is approached rapidly if the initial value of $h^2(\Lambda)/\Lambda$ is large enough, i.e. in the broad-resonance limit. Then the memory of the microscopic value of $h^2(\Lambda)/\Lambda$ is lost at large length

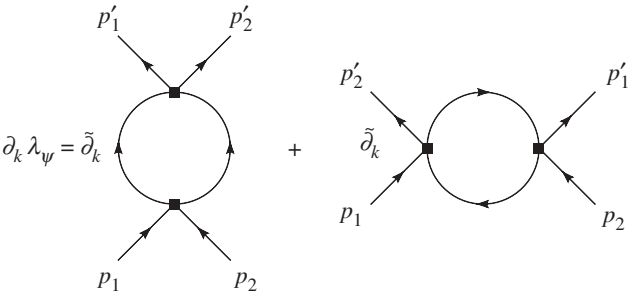

Figure 2. Running of the momentum-dependent vertex λ_ψ. Here, $\tilde{\partial}_k$ indicates scale derivatives with respect to the regulator in the propagators but does not act on the vertices.

scales. Also, all other parameters except for the mass term m^2 are attracted to IR fixed points, giving rise to universality. The fixed-point structure remains similar for non-vanishing density and temperature, and these findings also apply in this regime and determine the critical physics of these non-relativistic quantum fields. For a given temperature, this fixed point has only one relevant direction, which is related to the detuning of the resonance, $B - B_0$.

4. Particle–hole fluctuations

(*a*) *Gorkov's correction to Bardeen–Cooper–Schrieffer theory*

For small and negative scattering length $c^{-1} < 0, |c| \ll 1$ (BCS side), the system can be treated by the perturbative BCS theory of superfluidity [40,41]. However, there is a significant decrease of the critical temperature when compared with the original BCS result owing to a screening effect of ph fluctuations in the medium [42,43]. Here, we will sketch the technique to include the effect of ph fluctuations in our functional RG treatment as developed by Floerchinger *et al.* [30].

In an RG setting, the features of BCS theory can be described in a purely fermionic language, with the fermion interaction vertex λ_ψ as the only scale-dependent object. In general, the interaction vertex is momentum-dependent, $\lambda_\psi(p_1', p_1, p_2', p_2)$, and its flow has two contributions that are depicted in figure 2, including the external momentum labels. For $k \to 0,\ \mu \to 0,\ T \to 0$ and $n \to 0$, this coupling is related to the scattering length, $a = (1/8\pi)\lambda_\psi(p_i = 0)$.

In the BCS approximation only the first diagram in figure 2, the particle–particle (pp) loop, is kept and the momentum dependence of the four-fermion coupling is neglected, by replacing $\lambda_\psi(p_1', p_1, p_2', p_2)$ with the point-like coupling evaluated at zero momentum. For $\mu > 0$, its effect increases as the temperature T is lowered. For small temperatures $T \leq T_{\mathrm{c,BCS}}$, the logarithmic divergence leads to the appearance of pairing, as $\lambda_\psi \to \infty$, corresponding to a pole in the four-point correlator. In terms of the scattering length a, Fermi momentum k_F and Fermi temperature T_F, the critical temperature is found to be

$$T_{\mathrm{c,BCS}} \approx 0.61\, T_\mathrm{F}\, \mathrm{e}^{\pi/(2ak_\mathrm{F})}. \tag{4.1}$$

At zero temperature, the expression for the second diagram in figure 2, the ph loop, vanishes if it is evaluated for vanishing external momenta, as both poles of the frequency integration are always in either the upper or lower half of the

complex plane. The dominant part of the scattering in a fermion gas occurs, however, for momenta on the Fermi surface rather than for zero momentum. For non-zero momenta of the external particles, the ph loop makes an important contribution. Setting the external frequencies to zero, we find that the inverse propagators in the ph loop are

$$P_\psi(q) = \mathrm{i}q_0 + (\boldsymbol{q} - \boldsymbol{p}_1)^2 - \mu \quad \text{and} \quad P_\psi(q) = \mathrm{i}q_0 + (\boldsymbol{q} - \boldsymbol{p}_2')^2 - \mu. \tag{4.2}$$

Depending on the value of the momenta $\boldsymbol{p}_1$ and $\boldsymbol{p}_2'$, there are now values of the loop momentum $\boldsymbol{q}$ for which the poles of the frequency integration are in different half-planes so that there is a non-zero contribution even for $T = 0$.

To include the effect of ph fluctuations, one could take the full momentum dependence of the vertex λ_ψ into account. However, the resulting integro-differential equations represent a substantial numerical challenge. As a simple and efficient approximation, one therefore restricts the flow to the running of a single coupling λ_ψ by choosing an appropriate momentum projection.

The averaging prescription used by Gorkov & Melik-Barkhudarov [42] leads to

$$T_\mathrm{c} = \frac{1}{(4\mathrm{e})^{1/3}}\, T_{\mathrm{c,BCS}} \approx \frac{1}{2.2}\, T_{\mathrm{c,BCS}} \tag{4.3}$$

and similar for the gap Δ at zero temperature.

(*b*) *Scale-dependent bosonization*

In §2 we describe an effective four-fermion interaction by the exchange of a boson. In this picture, the phase transition to the superfluid phase is indicated by the vanishing of the bosonic 'mass term' $m^2 = 0$. Negative m^2 leads to the spontaneous breaking of U(1) symmetry, as the minimum of the effective potential occurs for a non-vanishing superfluid density, $\rho_0 > 0$.

For $m^2 \geq 0$, we can solve the field equation for the boson ϕ as a functional of ψ and insert the solution into the effective action. This leads to an effective four-fermion vertex describing the scattering $\psi_1(p_1)\psi_2(p_2) \to \psi_1(p_1')\psi_2(p_2')$,

$$\lambda_{\psi,\mathrm{eff}} = \frac{-h^2}{\mathrm{i}(p_1 + p_2)_0 + \frac{1}{2}(\boldsymbol{p}_1 + \boldsymbol{p}_2)^2 + m^2}. \tag{4.4}$$

To investigate the breaking of U(1) symmetry and the onset of superfluidity, we first consider the flow of the bosonic propagator, which is mainly driven by the fermionic loop diagram. For the effective four-fermion interaction, this accounts for the pp loop (figure 3*a*,*b*). In the BCS limit of a large microscopic m_Λ^2, the running of m^2 for $k \to 0$ reproduces the BCS result [40,41].

The ph fluctuations are not accounted for by the renormalization of the boson propagator. Indeed, we have neglected so far that a four-fermion interaction term λ_ψ in the effective action is generated by the flow. This holds even if the microscopic point-like interaction is absorbed by a Hubbard–Stratonovich transformation into an effective boson exchange, such that $\lambda_\psi(\Lambda) = 0$. The strength of the total interaction between fermions,

$$\lambda_{\psi,\mathrm{eff}} = \frac{-h^2}{\mathrm{i}(p_1 + p_2)_0 + \frac{1}{2}(\boldsymbol{p}_1 + \boldsymbol{p}_2)^2 + m^2} + \lambda_\psi, \tag{4.5}$$

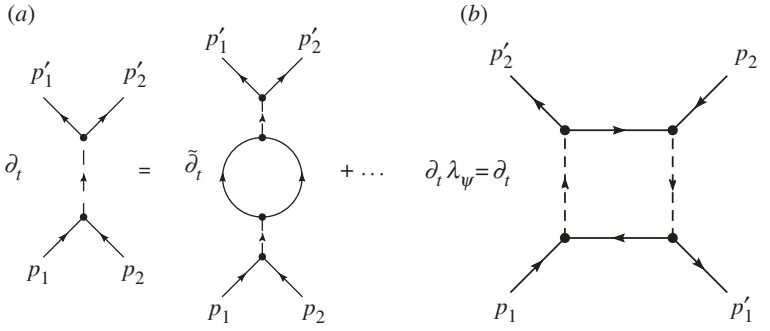

Figure 3. (*a*) Flow of the boson propagator. (*b*) Box diagram for the flow of the four-fermion interaction.

adds λ_ψ to the piece generated by boson exchange. In the partially bosonized formulation, the flow of λ_ψ is generated by the box diagrams depicted in figure 3*b*. A direct connection to the ph diagrams of figure 2 can be established on the BCS side and in the microscopic regime: there the boson gap m^2 is large. In this case, the effective fermion interaction in equation (4.5) becomes momentum independent, diagrammatically corresponding to a contracted bosonic propagator. The box diagram in figure 3 is then equivalent to the ph loop investigated in the last section, with the point-like approximation $\lambda_{\psi,\mathrm{eff}} \to -(h^2/m^2)$ for the fermion interaction vertex.

In contrast to the pp fluctuations (leading to spontaneous symmetry breaking for decreasing T), the ph fluctuations lead only to quantitative corrections and depend only weakly on temperature. This can be checked explicitly in the point-like approximation, and holds not only in the BCS regime where $T/\mu \ll 1$, but also for moderate T/μ as realized at the critical temperature in the unitary regime. We therefore evaluate the box diagrams in figure 2 for zero temperature. We emphasize that a temperature dependence, resulting from the couplings parametrizing the boson propagator, is implicitly taken into account. For the external momenta, we use an averaging on the Fermi surface similar to the one of Gorkov & Melik-Barkhudarov [42]. For details see Floerchinger *et al.* [30].

After these preliminaries, we can now incorporate the effect of ph fluctuations in the RG flow. In principle, one could simply take λ_ψ as an additional coupling into account. However, it is much more elegant to use a scale-dependent Hubbard–Stratonovich transformation [36,44,45], which absorbs λ_ψ into the Yukawa-type interaction with the bosons at every scale k. By construction, there is then no self-interaction between the fermionic quasiparticles. The general procedure of 'partial bosonization' is discussed in detail in Floerchinger *et al.* [30]. A slightly modified scheme based on the exact flow equation derived in Floerchinger & Wetterich [45] has been used in Floerchinger *et al.* [31]. In that formulation, one finds for the renormalized coupling m^2 in the symmetric regime an additional term reflecting the absorption of λ_ψ into the fermionic interaction induced by boson exchange,

$$\partial_t m^2 = \partial_t m^2 \Big|_{\mathrm{HS}} + \frac{m^4}{h^2} \partial_t \lambda_\psi \Big|_{\mathrm{HS}}. \tag{4.6}$$

Here $\partial_t m^2|_{\rm HS}$ and $\partial_t \lambda_\psi|_{\rm HS}$ denote the flow equations when the Hubbard–Stratonovich transformation is kept fixed. Since λ_ψ now remains zero during the flow, the effective four-fermion interaction $\lambda_{\psi,\rm eff}$ is purely given by the boson exchange. However, the contribution of the ph exchange diagrams is incorporated via the second term in equation (4.6). The flow equations of all other couplings are the same as with fixed Hubbard–Stratonovich transformation. In the regime with spontaneous symmetry breaking, we use

$$\left.\begin{aligned}\partial_t h &= \partial_t h\Big|_{\rm HS} + \frac{\lambda\rho_0}{h}\partial_t\lambda_\psi\Big|_{\rm HS},\\ \partial_t\rho_0 &= \partial_t\rho_0\Big|_{\rm HS} - 2\frac{\lambda\rho_0^2}{h^2}\partial_t\lambda_\psi\Big|_{\rm HS}\\ \text{and}\qquad \partial_t\lambda &= \partial_t\lambda\Big|_{\rm HS} + 2\frac{\lambda^2\rho_0}{h^2}\partial_t\lambda_\psi\Big|_{\rm HS}.\end{aligned}\right\} \tag{4.7}$$

We emphasize that our non-perturbative flow equations go beyond the treatment by Gorkov & Melik-Barkhudarov [42], which includes the ph diagrams only in a perturbative way. Furthermore, the inner bosonic lines $h^2/P_\phi(q)$ in the box diagrams include the centre-of-mass momentum dependence of the four-fermion vertex. This is neglected in Gorkov's point-like treatment, and thus represents a further improvement of the classic calculation. Actually, this momentum dependence becomes substantial away from the BCS regime, where the physics of the bosonic bound state sets in. The continuous description of dynamically transmuting degrees of freedom is a particular strength of an RG description, as exemplified also in the context of quantum chromodynamics [46,47].

5. Running Fermion sector

In this section, we aim at a systematic extension of the truncation scheme and consider a running fermion sector. Similar parametrizations of the fermionic self-energy have been studied in Gubbels & Stoof [24], Bartosch *et al.* [25] and Strack *et al.* [48]. Further, we include an atom–dimer interaction term. This section is based on the work by Floerchinger *et al.* [31].

(*a*) *Completion of the truncation*

In addition to the running couplings that have occurred so far in §3, now we want to take into account k-dependent parameters $\bar{m}_\psi^2$ and Z_ψ, in order to parametrize fluctuation effects on the self-energy of the fermionic quasiparticles. At the UV scale $k=\Lambda$, we use the initialization $\bar{m}_\psi^2=-\mu$ and $Z_\psi=1$. The extension of the truncation explicitly reads

$$\begin{aligned}\Gamma_k = \int_0^{1/T}\mathrm{d}\tau\int d^3x\,\Big\{&\bar\psi^\dagger Z_\psi(\partial_\tau-\nabla^2)\bar\psi + \bar m_\psi^2\bar\psi^\dagger\bar\psi + \bar\phi^*\left(\bar Z_\phi\partial_\tau - \frac{1}{2}A_\phi\nabla^2\right)\bar\phi\\ &+\ \bar U(\bar\rho,\mu) - \bar h(\bar\phi^*\bar\psi_1\bar\psi_2 + \bar\phi\bar\psi_2^*\bar\psi_1^*) + \bar\lambda_{\phi\psi}\bar\phi^*\bar\phi\bar\psi^\dagger\bar\psi\Big\}.\end{aligned} \tag{5.1}$$

The additional inclusion of the atom–dimer coupling $\bar{\lambda}_{\phi\psi}$ closes the truncation on the level of interaction terms quartic in the fields and describes three-body scattering [49]. It leads to quantitative modifications for the many-body problem. In the regime of spontaneously broken symmetry ($\rho_0 > 0$), the atom–dimer coupling leads to a modification of the Fermi surface, in addition to the gap $\sqrt{h^2\rho_0}$. We discuss this in more detail below.

We define the renormalized fields $\phi = A_\phi^{1/2}\bar{\phi}$, $\rho = A_\phi\bar{\rho}$, $\psi = Z_\psi^{1/2}\bar{\psi}$ and study the flow of the renormalized couplings $Z_\phi = \bar{Z}_\phi/A_\phi$, $h = \bar{h}/(A_\phi^{1/2}Z_\psi)$, $\lambda_{\phi\psi} = \bar{\lambda}_{\phi\psi}/(A_\phi Z_\psi)$, $m_\psi^2 = \bar{m}_\psi^2/Z_\psi$. As before, we expand the effective potential in monomials of ρ (see equation (3.3)). We use again a purely space-like regulator, which is adjusted to the running Fermi surface,

$$R_{k,\psi} = Z_\psi[\mathrm{sign}(\boldsymbol{p}^2 - r_\mathrm{F}^2)k^2 - (\boldsymbol{p}^2 - r_\mathrm{F}^2)]\theta(k^2 - |\boldsymbol{p}^2 - r_\mathrm{F}^2|)$$

and

$$R_{k,\phi} = A_\phi\left(k^2 - \frac{\boldsymbol{p}^2}{2}\right)\theta\left(k^2 - \frac{\boldsymbol{p}^2}{2}\right),$$

where $r_\mathrm{F}^2 = -m_\psi^2 - \lambda_{\phi\psi}\rho_0$. For the fermions, it regularizes fluctuations around the running Fermi surface, while for the bosons, fluctuations with small momenta are suppressed.

As a first quantity, we investigate the vacuum dimer–dimer scattering length a_M expressed in units of the atom–atom scattering length a. On the BEC side of the resonance, we can derive this quantity from the corresponding couplings by the equation

$$\frac{a_\mathrm{M}}{a} = 2\frac{\lambda}{\lambda_{\psi,\mathrm{eff}}}, \quad \lambda_{\psi,\mathrm{eff}} = 8\pi a = \frac{8\pi}{\sqrt{-\mu}}, \text{ for } \mu < 0 \text{ and } k = 0. \tag{5.2}$$

To explicitly compute the vacuum quantity a_M/a, we choose a value for a on the far BEC side, where for broad resonances the identity $a = (-\mu)^{-1/2}$ holds. We evolve the flow of the couplings to the IR and extract the value of λ, completely fixing a_M/a. In this truncation, including the $\lambda_{\phi\psi}$ vertex, we find $a_\mathrm{M}/a = 0.59$, which is in very good agreement with the well-known result from a direct solution of the Schrödinger equation, $a_\mathrm{M}/a = 0.60$ [50]. The accuracy of this result is somewhat surprising as no momentum dependence of $\lambda_{\phi\psi}$ has been taken into account. The latter has turned out to be important for the atom–dimer scattering [49]. On the other hand, the general leading-order effect of fermionic momentum dependence is captured by the wave function renormalization Z_ψ, the effect of which is largest in the strongly interacting regime, when $|c^{-1}| < 1$ (cf. figure 4).

(*b*) *Fermi sphere and dispersion relation*

The dispersion relation can be computed from the determinant of the renormalized fermionic propagator,

$$G_\psi^{-1} = \begin{pmatrix} -h\phi_0\epsilon & -\omega - (\boldsymbol{q}^2 + m_\psi^2 + \lambda_{\phi\psi}\rho_0) \\ -\omega + (\boldsymbol{q}^2 + m_\psi^2 + \lambda_{\phi\psi}\rho_0) & h\phi_0\epsilon \end{pmatrix}, \tag{5.3}$$

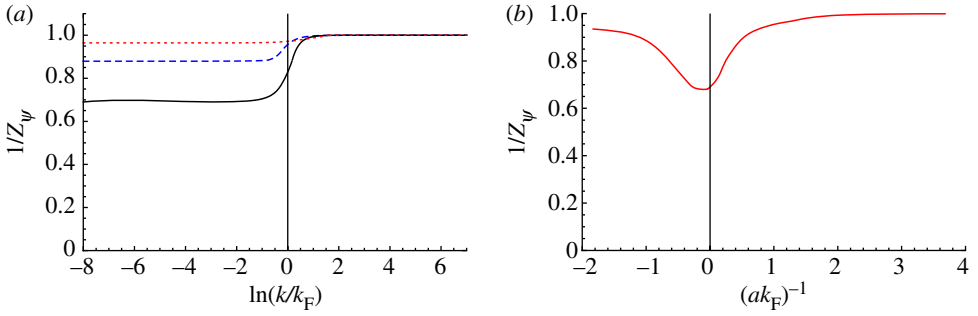

Figure 4. (*a*) Flow of the inverse fermionic wave function renormalization $1/Z_\psi$ at $T=0$ at three different points of the crossover: $c^{-1}=-1$ (dashed line), $c^{-1}=0$ (solid line), $c^{-1}=1$ (short dashed line). (*b*) Inverse fermionic wave function renormalization $1/Z_\psi$ at $k=0$ as a function of the crossover parameter c^{-1}. (Online version in colour.)

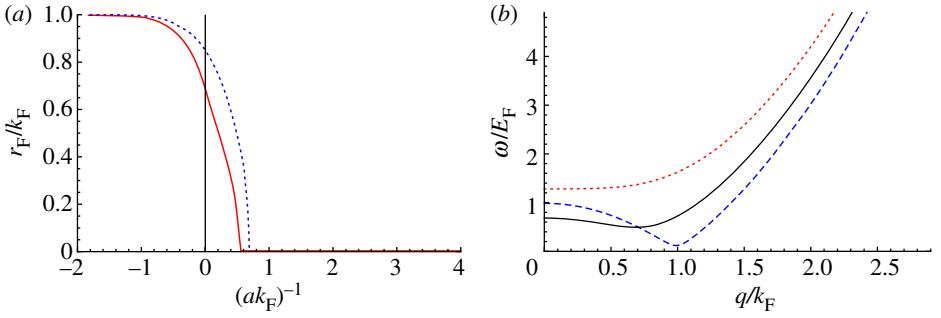

Figure 5. (*a*) Effective Fermi radius r_F/k_F as a function of the crossover parameter c^{-1} for vanishing temperature (solid line). We compare with the effective Fermi radius in an approximation without the contribution of the atom–dimer vertex $\lambda_{\phi\psi}$ (dotted line). (*b*) Positive branch of the dispersion relation $\omega(q)$ in units of E_F for $c^{-1}=-1$ (dashed), $c^{-1}=0$ (solid) and $c^{-1}=1$ (short dashed). (Online version in colour.)

by the equation $\det G_\psi^{-1}=0$. Here, we have evaluated G_ψ^{-1} in the regime of spontaneously broken symmetry and performed analytical continuation to real frequencies ω. We see that the dispersion relation is affected by the running of the couplings Z_ψ, m_ψ^2 and $\lambda_{\phi\psi}$, which follows as $\omega=\pm\sqrt{\Delta^2+(\boldsymbol{q}^2-r_F^2)^2}$, where $\Delta=h\sqrt{\rho_0}$ is the gap and $r_F=\sqrt{-m_\psi^2-\lambda_{\phi\psi}\rho_0}$ is the effective radius of the Fermi sphere. We note that r_F is defined by our parametrization of the dispersion relation for fermionic quasiparticles within the derivative expansion. It should not be confused with the quantity k_F related to the particle number density by equation (1.1). Only on the far BCS side of the crossover, the renormalization effects on r_F are small and r_F approaches its classical value $r_F\simeq\sqrt{\mu}=k_F$. Close to the resonance, the Fermi sphere gets smaller. It finally vanishes on the BEC side at a point with $c^{-1}\approx 0.6$ (figure 5). Here, the fermions are gapped even for $\Delta\to 0$ by a positive value of $m_\psi^2+\lambda_{\phi\psi}\rho_0$.

6. Results

For the studies in §5, we have omitted the effect of ph fluctuations for simplicity. In the following, however, all the results are given for the correspondingly extended truncation including ph fluctuations.

(a) *Single-particle gap at* $T = 0$

As a first study including all the couplings introduced in this contribution, we investigate the single-particle gap at zero temperature. On the far BCS side, it is possible to compare with the results of Gorkov & Melik-Barkhudarov [42], which is given by $\Delta/E_\mathrm{F} = (2/\mathrm{e})^{7/3}\mathrm{e}^{\pi/(2c)}$. Our approach allows one to extend to the strongly interacting regime and even to the BEC side of the crossover (figure 6). At the unitary point, $(ak_\mathrm{F})^{-1} = 0$, we obtain $\Delta/E_\mathrm{F} = 0.46$. Further, we compare our result for chemical potential in units of the Fermi energy at the unitary point $\mu/E_\mathrm{F} = 0.51$ with different (non-perturbative) methods in table 1.

(b) *Phase diagram*

Our results for the critical temperature for the phase transition to superfluidity throughout the crossover are shown in figure 6. We plot the critical temperature in units of the Fermi temperature $T_\mathrm{c}/T_\mathrm{F}$ as a function of the scattering length $c = ak_\mathrm{F}$ measured in units of the inverse Fermi momentum.

On the BCS side of the crossover, where $c^{-1} \ll -1$, the BCS approximation and the effect of ph fluctuations yield a critical temperature [42]

$$\frac{T_\mathrm{c}}{T_\mathrm{F}} = \frac{\mathrm{e}^C}{\pi}\left(\frac{2}{\mathrm{e}}\right)^{7/3}\mathrm{e}^{\pi/(ak_\mathrm{F})} \approx 0.28\mathrm{e}^{\pi/(ak_\mathrm{F})}, \tag{6.1}$$

depicted by the short dashed line in figure 6*b*. Here, $C \approx 0.577$ is Euler's constant. On the BEC side for very large and positive c^{-1}, our result approaches the critical temperature of a free Bose gas where the bosons have twice the mass of the fermions, $M_\mathrm{B} = 2M$. In our units, the critical temperature is then

$$\frac{T_\mathrm{c,BEC}}{T_\mathrm{F}} = \frac{2\pi}{(6\pi^2\zeta(3/2))^{2/3}} \approx 0.218. \tag{6.2}$$

In between there is the unitarity regime, where the two-atom scattering length diverges ($c^{-1} \to 0$) and we deal with a system of strongly interacting fermions.

Our best result including ph fluctuations is given by the solid line. This may be compared with a functional renormalization flow investigation ignoring ph fluctuations as discussed in §3 (dot-dashed line) [22]. For $c \to 0_-$, the solid line of our result agrees with the BCS theory including the correction by Gorkov & Melik-Barkhudarov [42]. Deviations from this perturbative regime appear only rather close to the regime of strong interactions, $c^{-1} \to 0$.

For $c \to 0_+$, this value is approached in the form [51]

$$\frac{T_\mathrm{c} - T_\mathrm{c,BEC}}{T_\mathrm{c,BEC}} = \kappa a_\mathrm{M} n_\mathrm{M}^{1/3} = \kappa\frac{a_\mathrm{M}}{a}\frac{c}{(6\pi^2)^{1/3}}. \tag{6.3}$$

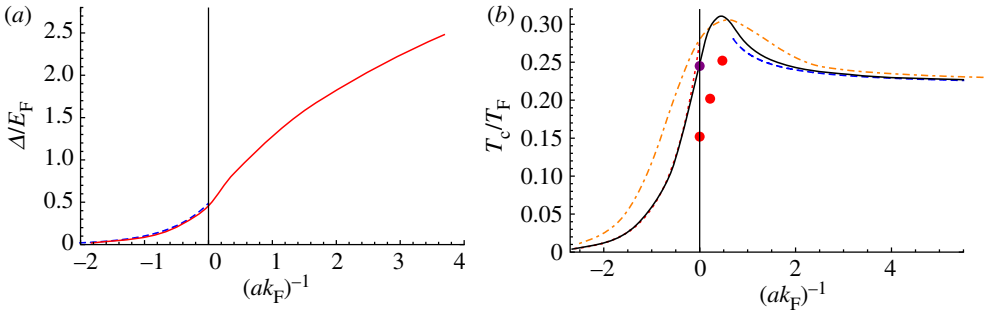

Figure 6. (*a*) Gap in units of the Fermi energy Δ/E_F as a function of $(ak_F)^{-1}$ (solid line). For comparison, we also plot the results found by Gorkov & Melik-Barkhudarov (dashed) and extrapolate this to the unitary point $(ak_F)^{-1}=0$, where $\Delta_{GMB}/E_F=0.49$. (*b*) Critical temperature T_c/T_F in units of the Fermi temperature as a function of the crossover parameter $(ak_F)^{-1}$. The solid line gives the result of our full computation referred to in the text. The dot-dashed line is obtained using the more basic truncation discussed in §3. The dotted line shown for $(ak_F)^{-1}<0$ shows the result of the perturbative calculation by Gorkov & Melik-Barkhudarov [42]. The dashed line corresponds to an interacting BEC with the shift in T_c according to equation (6.3). We use here $a_M/a=0.60$ and $\kappa=1.31$. The three red dots close to and at unitarity show the QMC results by Burovski *et al.* [15], while the single purple dot gives the result of Akkineni *et al.* [16]. (Online version in colour.)

Table 1. Results for the single-particle gap and the chemical potential at $T=0$ and at the unitary point by various authors.

	μ/E_F	Δ/E_F
Carlson *et al.* [12] (QMC)	0.43	0.54
Perali *et al.* [18] (*t*-matrix approach)	0.46	0.53
Haussmann *et al.* [20] (2PI)	0.36	0.46
Bartosch *et al.* [25] (functional RG, vertex exp.)	0.32	0.61
Floerchinger *et al.* [31] (functional RG, derivative exp.)	0.51	0.46

Here, $n_M=n/2$ is the density of molecules and a_M is the molecular scattering length. Using our result $a_M/a=0.59$ obtained from solving the flow equations in vacuum, the coefficient determining the shift in T_c compared with the free Bose gas yields $\kappa=1.39$ (see also [22]). In Arnold & Moore [52] and Kashurnikov *et al.* [53], the result for an interacting BEC is determined as $\kappa=1.31$ (dashed curve on BEC side of figure 6*b*) see also [54,55] for a functional RG study. This is in reasonable agreement with our result. As further characteristic quantities we give the maximum of the ratio $(T_c/T_F)_{max}\approx 0.31$ and the location of the maximum $(ak_F)^{-1}_{max}\approx 0.40$. For $c^{-1}>0.5$, the effect of the ph fluctuations vanishes. This is expected, as the chemical potential is now negative, $\mu<0$, such that the Fermi surface disappears.

In the unitary regime $(c^{-1}\approx 0)$, the ph fluctuations still have a quantitative effect. We can give an improved estimate for the critical temperature at the resonance $(c^{-1}=0)$, where we find $T_c/T_F=0.248$ and a chemical potential

Table 2. Results for T_c/T_F and μ_c/T_F at the unitary point by various authors.

	μ_c/E_F	T_c/T_F
Burovski *et al.* [15] (QMC)	0.49	0.15
Bulgac *et al.* [14] (QMC)	0.43	<0.15
Akkineni *et al.* [16] (QMC)	–	0.245
Previous functional RG estimate by Floerchinger *et al.* [30]	0.68	0.276
Floerchinger *et al.* [31] (functional RG)	0.55	0.248

$\mu_c/T_F = 0.55$. A comparison with other methods and our previous work is given in table 2. We observe reasonable agreement with QMC results for the chemical potential μ_c/T_F; however, our critical temperature T_c/T_F is larger.

7. Discussion and outlook

As illustrated with the example of the BCS–BEC crossover, the functional RG is capable of describing strongly interacting many-body systems in a consistent and controllable fashion. Once the relevant degrees of freedom are identified—possibly in a scale-dependent manner—approximation schemes based on expansions of the effective action can be devised that facilitate systematically improvable quantitative estimates of physical observables. For the BCS–BEC crossover, already a simple derivative expansion including fermionic and composite bosonic degrees of freedom exhibits all qualitative features of the phase diagram. New insights are provided by the RG by associating universal aspects of the phenomena with a fixed-point structure of the flow.

The inclusion of ph fluctuations and higher orders of the derivative expansion improve our numerical results in the BCS as well as in the BEC limit of the crossover, in agreement with the other well-known field-theoretical methods. We obtain satisfactory quantitative precision on the BCS and BEC sides of the resonance. Remarkably, the functional RG allows for a description of both many-body as well as few-body physics within the same formalism. For instance, our result for the molecular scattering length ratio a_M/a is in good agreement with the exact result [50]. This quantitative accuracy is remarkable, as we have started with a purely fermionic microscopic theory without propagating bosonic degrees of freedom or bosonic interactions.

In the strongly interacting regime where the scattering length diverges, no exact analytical treatments are available. Our results for the gap Δ/E_F and the chemical potential μ/E_F at zero temperature are in reasonable agreement with Monte Carlo simulations. This holds also for the ratio μ_c/E_F at the critical temperature. The critical temperature T_c/T_F itself is found to be larger than the Monte Carlo result.

In future studies, our approximations might be improved mainly at two points. One is the frequency and momentum dependence of the boson propagator. In the strongly interacting regime, this might be rather involved, developing structures beyond our current approximation. A more detailed resolution might lead to modifications in the contributions from bosonic fluctuations to various flow equations. Another point concerns structures in the fermion–fermion interaction that go beyond a diatom bound-state exchange process. Close to the unitary

point, other contributions might arise, for example, in the form of a ferromagnetic channel. While further quantitative modifications in the unitarity regime are conceivable, the present approximation already allows for a coherent description of the BCS–BEC crossover for all values of the scattering length, temperature and density by one simple method and microscopic model. This includes the critical behaviour of a second-order phase transition as well as the vacuum, BEC and BCS limits.

In order to improve the comparison between the QMC simulations and the functional RG results in the strongly interacting regime, the Wetterich equation can also be evaluated in a finite volume. This may shed light on possible finite size effects in the QMC simulations, and can help to quantitatively compare finite-volume studies with infinite-volume calculations inherent to most analytical works.

The authors are grateful to J. Braun, S. Diehl, J. M. Pawlowski and C. Wetterich for collaboration on the subject reviewed here. This work has been supported by the DFG research unit FOR 723. H.G. acknowledges support by the DFG under contract Gi 328/5-1 (Heisenberg programme). S.F. acknowledges support by the Helmholtz Alliance HA216/EMMI.

References

1 Eagles, D. M. 1969 Possible pairing without superconductivity at low carrier concentrations in bulk and thin-film superconducting semiconductors. *Phys. Rev.* **186**, 456–463. (doi:10.1103/PhysRev.186.456)
2 Leggett, A. J. 1980 Diatomic molecules and Cooper pairs. In *Modern trends in the theory of condensed matter* (ed. A. Pekalski and R. Przystawa), pp. 13–27. Berlin, Germany: Springer.
3 O'Hara, K. M., Hemmer, S. L., Granade, S. R., Gehm, M. E., Thomas, J. E., Venturi, V., Tiesinga, E. & Williams, C. J. 2002 Measurement of the zero crossing in a Feshbach resonance of fermionic ^{6}Li. *Phys. Rev. A* **66**, 041401(R). (doi:10.1103/PhysRevA.66.041401)
4 Regal, C. A., Greiner, M. & Jin, D. S. 2004 Observation of resonance condensation of fermionic atom pairs. *Phys. Rev. Lett.* **92**, 040403. (doi:10.1103/PhysRevLett.92.040403)
5 Zwierlein, M. W., Stan, C. A., Schunck, C. H., Raupach, S. M. F., Kerman, A. J. & Ketterle, W. 2004 Condensation of pairs of fermionic atoms near a Feshbach resonance. *Phys. Rev. Lett.* **92**, 120403. (doi:10.1103/PhysRevLett.92.120403)
6 Kinast, J., Hemmer, S. L., Gehm, M. E., Turlapov, A. & Thomas, J. E. 2004 Evidence for superfluidity in a resonantly interacting Fermi gas. *Phys. Rev. Lett.* **92**, 150402. (doi:10.1103/PhysRevLett.92.150402)
7 Bourdel, T. *et al.* 2004 Experimental study of the BEC–BCS crossover region in lithium 6. *Phys. Rev. Lett.* **93**, 050401. (doi:10.1103/PhysRevLett.93.050401)
8 Bartenstein, M., Altmeyer, A., Riedl, S., Jochim, S., Chin, C., Denschlag, J. H. & Grimm, R. 2004 Crossover from a molecular Bose–Einstein condensate to a degenerate Fermi gas. *Phys. Rev. Lett.* **92**, 120401. (doi:10.1103/PhysRevLett.92.120401)
9 Partridge, G. B., Strecker, K. E., Kamar, R. I., Jack, M. W. & Hulet, R. G. 2005 Molecular probe of pairing in the BEC–BCS crossover. *Phys. Rev. Lett.* **95**, 020404. (doi:10.1103/PhysRevLett.95.020404)
10 Nozieres, P. & Schmitt-Rink, S. 1985 Bose condensation in an attractive fermion gas: from weak to strong coupling superconductivity. *J. Low Temp. Phys.* **59**, 195–211. (doi:10.1007/BF00683774)
11 Sa de Melo, C. A. R., Randeria, M. & Engelbrecht, J. R. 1993 Crossover from BCS to Bose superconductivity: transition temperature and time-dependent Ginzburg–Landau theory. *Phys. Rev. Lett.* **71**, 3202–3205. (doi:10.1103/PhysRevLett.71.3202)
12 Carlson, J., Chang, S. Y., Pandharipande, V. R. & Schmidt, K. E. 2003 Superfluid Fermi gases with large scattering length. *Phys. Rev. Lett.* **91**, 050401. (doi:10.1103/PhysRevLett.91.050401)

13 Astrakharchik, G. E., Boronat, J., Casulleras, J. & Giorgini, S. 2004 Equation of state of a Fermi gas in the BEC–BCS crossover: a quantum Monte Carlo study. *Phys. Rev. Lett.* **93**, 200404. (doi:10.1103/PhysRevLett.93.200404)
14 Bulgac, A., Drut, J. E. & Magierski, P. 2006 Spin 1/2 fermions in the unitary regime: a superfluid of a new type. *Phys. Rev. Lett.* **96**, 090404. (doi:10.1103/PhysRevLett.96.090404)
15 Burovski, E., Prokof'ev, N., Svistunov, B. & Troyer, M. 2006 Critical temperature and thermodynamics of attractive fermions at unitarity. *Phys. Rev. Lett.* **96**, 160402. (doi:10.1103/PhysRevLett.96.160402)
16 Akkineni, V. K., Ceperley, D. M. & Trivedi, N. 2007 Pairing and superfluid properties of dilute fermion gases at unitarity. *Phys. Rev. B* **76**, 165116. (doi:10.1103/PhysRevB.76.165116)
17 Pieri, P. & Strinati, G. C. 2000 Strong-coupling limit in the evolution from BCS superconductivity to Bose–Einstein condensation. *Phys. Rev. B* **61**, 15 370–15 381. (doi:10.1103/PhysRevB.61.15370)
18 Perali, A., Pieri, P., Pisani, L. & Strinati, G. C. 2004 BCS–BEC crossover at finite temperature for superfluid trapped Fermi atoms. *Phys. Rev. Lett.* **92**, 220404. (doi:10.1103/PhysRevLett.92.220404)
19 Diehl, S. & Wetterich, C. 2006 Universality in phase transitions for ultracold fermionic atoms. *Phys. Rev. A* **73**, 033615. (doi:10.1103/PhysRevA.73.033615)
20 Haussmann, R., Rantner, W., Cerrito, S. & Zwerger, W. 2007 Thermodynamics of the BCS–BEC crossover. *Phys. Rev. A* **75**, 023610. (doi:10.1103/PhysRevA.75.023610)
21 Birse, M. C., Krippa, B., McGovern, J. A. & Walet, N. R. 2005 Pairing in many-fermion systems: an exact renormalisation group treatment. *Phys. Lett. B* **605**, 287–294. (doi:10.1016/j.physletb.2004.11.044)
22 Diehl, S., Gies, H., Pawlowski, J. M. & Wetterich C. 2007 Flow equations for the BCS–BEC crossover. *Phys. Rev. A* **76**, 021602(R). (doi:10.1103/PhysRevA.76.021602)
23 Diehl, S., Gies, H., Pawlowski, J. M. & Wetterich, C. 2007 Renormalisation flow and universality for ultracold fermionic atoms. *Phys. Rev. A* **76**, 053627. (doi:10.1103/PhysRevA.76.053627)
24 Gubbels, K. B. & Stoof, H. T. C. 2008 Renormalization group theory for the imbalanced Fermi gas. *Phys. Rev. Lett.* **100**, 140407. (doi:10.1103/PhysRevLett.100.140407)
25 Bartosch, L., Kopietz, P. & Ferraz, A. 2009 Renormalization of the BCS–BEC crossover by order parameter fluctuations. *Phys. Rev. B* **80**, 104514. (doi:10.1103/PhysRevB.80.104514)
26 Krippa, B. 2009 Exact renormalisation group flow for ultracold Fermi gases in unitary limit. *J. Phys. A* **42**, 465002. (doi:10.1088/1751-8113/42/46/465002)
27 Nikolic, P. & Sachdev, S. 2007 Renormalization-group fixed points, universal phase diagram, and $1/N$ expansion for quantum liquids with interactions near the unitarity limit. *Phys. Rev. A* **75**, 033608. (doi:10.1103/PhysRevA.75.033608)
28 Ho, T. L. 2004 Universal thermodynamics of degenerate quantum gases in the unitarity limit. *Phys. Rev. Lett.* **92**, 090402. (doi:10.1103/PhysRevLett.92.090402)
29 Diehl, S., Floerchinger, S., Gies, H., Pawlowski, J. M. & Wetterich, C. 2010 Functional renormalization group approach to the BCS–BEC crossover. *Annalen Phys.* **522**, 615–656. (doi:10.1002/andp.201010458)
30 Floerchinger, S., Scherer, M., Diehl, S. & Wetterich, C. 2009 Particle–hole fluctuations in the BCS–BEC crossover. *Phys. Rev. B* **78**, 174528. (doi:10.1103/PhysRevB.78.174528)
31 Floerchinger, S., Scherer, M. M. & Wetterich, C. 2010 Modified Fermi-sphere, pairing gap and critical temperature for the BCS–BEC crossover. *Phys. Rev. A* **81**, 063619. (doi:10.1103/PhysRevA.81.063619)
32 Wetterich, C. 1993 Exact evolution equation for the effective potential. *Phys. Lett. B* **301**, 90–94. (doi:10.1016/0370-2693(93)90726-X)
33 Salmhofer, M. & Honerkamp, C. 2001 Fermionic renormalization group flows: technique and theory. *Prog. Theor. Phys.* **105**, 1–35. (doi:10.1143/PTP.105.1)
34 Berges, J., Tetradis, N. & Wetterich, C. 2002 Non-perturbative renormalization flow in quantum field theory and statistical physics. *Phys. Rep.* **363**, 223–386. (doi:10.1016/S0370-1573(01)00098-9)

35 Gies, H. 2006 Introduction to the functional RG and applications to gauge theories. Lecture given at 2006 ECT School, Trento, Italy. (http://arxiv.org/abs/hep-ph/0611146)

36 Pawlowski, J. M. 2007 Aspects of the functional renormalisation group. *Annals Phys.* **322**, 2831–2915. (doi:10.1016/j.aop.2007.01.007)

37 Kopietz, P., Bartosch, L. & Schutz, F. 2010 *Introduction to the functional renormalization group.* Lecture Notes in Physics, no. 798. Berlin, Germany: Springer. (doi:10.1007/978-3-642-05094-7)

38 Litim, D. F. 2000 Optimisation of the exact renormalisation group. *Phys. Lett. B* **486**, 92–99. (doi:10.1016/S0370-2693(00)00748-6)

39 Diehl, S. & Wetterich, C. 2007 Functional integral for ultracold fermionic atoms. *Nucl. Phys. B* **770**, 206–272. (doi:10.1016/j.nuclphysb.2007.02.026)

40 Cooper, L. N. 1956 Bound electron pairs in a degenerate Fermi gas. *Phys. Rev.* **104**, 1189–1190. (doi:10.1103/PhysRev.104.1189)

41 Bardeen, J., Cooper, L. N. & Schrieffer, J. R. 1957 Theory of superconductivity. *Phys. Rev.* **108**, 1175–1204. (doi:10.1103/PhysRev.108.1175)

42 Gorkov, L. P. & Melik-Barkhudarov T. K. 1962 Contribution to the theory of superfluidity in an imperfect Fermi gas. *Sov. Phys.–JETP* **13**, 1018–1022.

43 Heiselberg, H., Pethick, C. J., Smith, H. & Viverit, L. 2000 Influence of induced interactions on the superfluid transition in dilute Fermi gases. *Phys. Rev. Lett.* **85**, 2418–2421. (doi:10.1103/PhysRevLett.85.2418)

44 Gies, H. & Wetterich, C. 2002 Renormalization flow of bound states. *Phys. Rev. D* **65**, 065001. (doi:10.1103/PhysRevD.65.065001)

45 Floerchinger, S. & Wetterich, C. 2009 Exact flow equation for composite operators. *Phys. Lett. B* **680**, 371–376. (doi:10.1016/j.physletb.2009.09.014)

46 Gies, H. & Wetterich, C. 2004 Universality of spontaneous chiral symmetry breaking in gauge theories. *Phys. Rev. D* **69**, 025001. (doi:10.1103/PhysRevD.69.025001)

47 Braun J. 2009 The QCD phase boundary from quark–gluon dynamics. *Eur. Phys. J. C* **64**, 459–482. (doi:10.1140/epjc/s10052-009-1136-6)

48 Strack, P., Gersch, R. & Metzner, W. 2008 Renormalization group flow for fermionic superfluids at zero temperature. *Phys. Rev. B* **78**, 014522. (doi:10.1103/PhysRevB.78.014522)

49 Diehl, S., Krahl, H. C., & Scherer, M. 2008 Three-body scattering from non-perturbative flow equations. *Phys. Rev. C* **78**, 034001. (doi:10.1103/PhysRevC.78.034001)

50 Petrov, D. S., Salomon, C. & Shlyapnikov, G. V. 2004 Weakly bound dimers of fermionic atoms. *Phys. Rev. Lett.* **93**, 090404. (doi:10.1103/PhysRevLett.93.090404)

51 Baym, G., Blaizot, J. P., Holzmann, M., Laloe, F. & Vautherin, D. 1999 The transition temperature of the dilute interacting Bose gas. *Phys. Rev. Lett.* **83**, 1703–1706. (doi:10.1103/PhysRevLett.83.1703)

52 Arnold, P. & Moore, G. D. 2001 Transition temperature of a dilute homogeneous imperfect Bose gas. *Phys. Rev. Lett.* **87**, 120401. (doi:10.1103/PhysRevLett.87.120401)

53 Kashurnikov, V. A., Prokof'ev, N. V. & Svistunov, B. V. 2001 Critical temperature shift in weakly interacting Bose gas. *Phys. Rev. Lett.* **87**, 120402. (doi:10.1103/PhysRevLett.87.120402)

54 Blaizot, J. P., Méndez-Galain, R. & Wschebor, N. 2006 Nonperturbative renormalization group and momentum dependence of n-point functions. I. *Phys. Rev. E* **74**, 051116. (doi:10.1103/PhysRevE.74.051116)

55 Blaizot, J. P., Méndez-Galain, R. & Wschebor, N. 2006 Nonperturbative renormalization group and momentum dependence of n-point functions. II. *Phys. Rev. E* **74**, 051117. (doi:10.1103/PhysRevE.74.051117)